ARMY RESEARCH LABORATORY

Through-the-Wall Radar Simulations for Complex Room Imaging

by Traian Dogaru and Calvin Le

ARL-TR-5205 **May 2010**

Approved for public release; distribution unlimited.

NOTICES

Disclaimers

The findings in this report are not to be construed as an official Department of the Army position unless so designated by other authorized documents.

Citation of manufacturer's or trade names does not constitute an official endorsement or approval of the use thereof.

Destroy this report when it is no longer needed. Do not return it to the originator.

Army Research Laboratory
Adelphi, MD 20783-1197

ARL-TR-5205 **May 2010**

Through-the-Wall Radar Simulations for Complex Room Imaging

Traian Dogaru and Calvin Le
Sensors and Electron Devices Directorate, ARL

Approved for public release; distribution unlimited.

REPORT DOCUMENTATION PAGE	Form Approved OMB No. 0704-0188

Public reporting burden for this collection of information is estimated to average 1 hour per response, including the time for reviewing instructions, searching existing data sources, gathering and maintaining the data needed, and completing and reviewing the collection information. Send comments regarding this burden estimate or any other aspect of this collection of information, including suggestions for reducing the burden, to Department of Defense, Washington Headquarters Services, Directorate for Information Operations and Reports (0704-0188), 1215 Jefferson Davis Highway, Suite 1204, Arlington, VA 22202-4302. Respondents should be aware that notwithstanding any other provision of law, no person shall be subject to any penalty for failing to comply with a collection of information if it does not display a currently valid OMB control number.
PLEASE DO NOT RETURN YOUR FORM TO THE ABOVE ADDRESS.

1. REPORT DATE *(DD-MM-YYYY)*	2. REPORT TYPE	3. DATES COVERED (From - To)
May 2010	Final	2008–2010

4. TITLE AND SUBTITLE	5a. CONTRACT NUMBER
Through-the-Wall Radar Simulations for Complex Room Imaging	5b. GRANT NUMBER
	5c. PROGRAM ELEMENT NUMBER
6. AUTHOR(S)	5d. PROJECT NUMBER
Traian Dogaru and Calvin Le	5e. TASK NUMBER
	5f. WORK UNIT NUMBER
7. PERFORMING ORGANIZATION NAME(S) AND ADDRESS(ES)	8. PERFORMING ORGANIZATION REPORT NUMBER
U.S. Army Research Laboratory ATTN: RDRL-SER-U 2800 Powder Mill Road Adelphi, MD 20783-1197	ARL-TR-5205
9. SPONSORING/MONITORING AGENCY NAME(S) AND ADDRESS(ES)	10. SPONSOR/MONITOR'S ACRONYM(S)
	11. SPONSOR/MONITOR'S REPORT NUMBER(S)

12. DISTRIBUTION/AVAILABILITY STATEMENT

Approved for public release; distribution unlimited.

13. SUPPLEMENTARY NOTES

14. ABSTRACT

This report demonstrates the application of synthetic aperture radar (SAR) techniques on imaging a complex room containing realistic features, such as doors, windows, interior walls, furniture objects, and humans. We analyze the changes in the radar phenomenology as we consider various aspect angles and polarizations. The scenarios investigated here correspond to either ground-based or airborne radar systems. Enhancements in the radar images can be obtained by combining images from different aspect angles. We demonstrate the advantages of using cross-polarization for detecting human targets. We also emphasize the importance of multipath propagation effects in interpreting radar images. All the numerical examples are based on radar data obtained through computer simulation of the electromagnetic (EM) scattering problems using either the finite-difference time-domain (FDTD) method or Xpatch. The accuracy of the EM modeling methods is evaluated by comparing the images based on FDTD and Xpatch simulations.

15. SUBJECT TERMS

Radar, sensing through the wall

16. SECURITY CLASSIFICATION OF:			17. LIMITATION OF ABSTRACT	18. NUMBER OF PAGES	19a. NAME OF RESPONSIBLE PERSON
a. REPORT	b. ABSTRACT	c. THIS PAGE			Traian Dogaru
Unclassified	Unclassified	Unclassified	UU	30	19b. TELEPHONE NUMBER (*Include area code*) (301) 394-1482

Standard Form 298 (Rev. 8/98)
Prescribed by ANSI Std. Z39.18

Contents

List of Figures **iv**

List of Tables **v**

Acknowledgments **vi**

1. Introduction **1**

2. Modeling Methods **2**

2.1 Electromagnetic Modeling 2

2.2 Computational Meshes 2

2.3 SAR Imaging Algorithm 4

3. Numerical Results **6**

3.1 SAR Images from a Ground-based Radar System 6

3.2 Using Cross-polarization for SAR Imaging 8

3.3 Combining SAR Images from Different Aspect Angles 8

3.4 SAR Images from an Airborne-based Radar System 10

3.5 Comparison between AFDTD and Xpatch Models 13

4. Conclusions **17**

5. References **19**

List of Symbols, Abbreviations, and Acronyms **21**

Distribution List **22**

List of Figures

Figure 1. Complex room containing humans and furniture objects showing the (a) perspective view and (b) top view. 3

Figure 2. Spotlight SAR geometry implemented by the models in this report, showing two possible aperture positions. 5

Figure 3. SAR images of the complex room, obtained for spotlight mode and PFA from AFDTD data in V-V polarization, 0° elevation, 1.1 GHz bandwidth centered at 1.4 GHz, for a 30° synthetic aperture placed on the (a) left side and (b) bottom side. 7

Figure 4. SAR images of the complex room, obtained for spotlight mode and PFA from AFDTD data in H-H polarization, 0° elevation, 1.1 GHz bandwidth centered at 1.4 GHz, for a 30° synthetic aperture placed on the (a) left side and (b) bottom side. 7

Figure 5. SAR images of the complex room, obtained for spotlight mode and PFA from AFDTD data in V-H polarization, 0° elevation, 1.1 GHz bandwidth centered at 1.4 GHz, for a 30° synthetic aperture placed on the (a) left side and (b) bottom side. 8

Figure 6. Incoherent pixel-by-pixel summation of the co-polarized images from both sides of the building showing (a) V-V and (b) V-H polarization. 9

Figure 7. Incoherent pixel-by-pixel summation of the V-V images from both sides of the building and the V-H image from (a) the left side of the building and (b) the bottom side of the building. 10

Figure 8. SAR images of the complex room, obtained for spotlight mode and PFA from AFDTD data in V-V polarization, 20° elevation, 1.1 GHz bandwidth centered at 1.4 GHz, for a 30° synthetic aperture placed on the (a) left side and (b) bottom side. 11

Figure 9. SAR images of the complex room, obtained for spotlight mode and PFA from AFDTD data in H-H polarization, 20° elevation, 1.1 GHz bandwidth centered at 1.4 GHz, for a 30° synthetic aperture placed on the (a) left side and (b) bottom side. 11

Figure 10. Composite SAR images of the complex room, obtained for spotlight mode and PFA from AFDTD data, 20° elevation, 1.1 GHz bandwidth centered at 1.4 GHz, scanning from two building sides with a 30° synthetic aperture, showing (a) V-V and (b) H-H polarization. 12

Figure 11. SAR images of the complex room, obtained for spotlight mode and PFA from AFDTD data in V-H polarization, 20° elevation, 1.1 GHz bandwidth centered at 1.4 GHz, for a 30° synthetic aperture placed on the (a) left side and (b) bottom side. 13

Figure 12. Composite SAR images of the complex room, obtained for spotlight mode and PFA, 0° elevation, 1.1 GHz bandwidth centered at 1.4 GHz, scanning from two building sides with a 30° synthetic aperture, showing (a) V-V polarization, AFDTD data; (b) H-H polarization, AFDTD data; (c) V-V polarization, Xpatch data; and (d) H-H polarization, Xpatch data. 14

Figure 13. Composite SAR images of the complex room, obtained for spotlight mode and PFA, 20° elevation, 1.1 GHz bandwidth centered at 1.4 GHz, scanning from two building sides with a 30° synthetic aperture, showing (a) V-V polarization, AFDTD data; (b) H-H polarization, AFDTD data; (c) V-V polarization, Xpatch data; and (d) H-H polarization, Xpatch data. 15

List of Tables

Table 1. Dielectric constant and conductivity of the materials involved in the complex room in figure 1. 3

Table 2. Comparison between AFDTD and Xpatch imaging results at the points highlighted in figure 12a for all the images considered in section 3.5 (data in dB). The bottom row contains the cross-correlation between the images created by the two methods. 16

Acknowledgments

This study was partially funded by the Communications-Electronics Research Development and Engineering Center (CERDEC), Intelligence and Information Warfare Directorate (I2WD) at Ft. Monmouth, NJ.

1. Introduction

The U.S. Army Research Laboratory (ARL) is currently supporting the Army's efforts in sensing through the wall (STTW) radar technology. One key component of these efforts is directed toward developing radar systems and signal processing algorithms for imaging complex building environments. The ARL contribution has consisted of radar system modeling and analysis (*1–3*), field measurements performed with the in-house-developed Synchronous Impulse Reconstruction (SIRE) radar (*4–5*), and signal processing techniques for behind-the-wall target detection (*6*). In terms of modeling, our emphasis has been on understanding the radar scattering phenomenology, developing image formation algorithms, and studying design parameter trade-offs, with the purpose of creating guidelines for optimized radar system performance.

In a previous study (*3*), we simulated a synthetic aperture radar (SAR) system for imaging a simple four-wall room with a human placed inside. Although that modeling scenario had a reduced complexity, it allowed us to understand a wealth of phenomenological effects that would be otherwise difficult to separate from a more complicated scene. Thus, we looked at the influence of radar parameters such as aperture size, frequency, bandwidth, and polarization on image quality. We also investigated different imaging techniques and algorithms as well as various construction materials. Finally, we made an accuracy assessment of the electromagnetic (EM) modeling methods employed in the radar scattering data generation.

In this report, we increase the complexity of the scene under investigation. Thus, we consider a large room, whose walls contain doors and windows. The interior includes furniture as well as humans. There is also an interior wall separating a small bedroom. All the objects in the computational mesh are obtained from very realistic computer aided design (CAD) models. The resulting computational space is very large, requiring powerful EM modeling software and hardware systems in order to obtain the radar signature over a wide range of aspect angles and frequencies.

Two possible types of radar platforms are simulated here: a ground-based platform and an airborne platform. Although we do not particularly emphasize new image formation algorithms, we discuss methods of combining images from different aspect angles and polarizations to enhance the building layout and/or the human targets in the SAR image domain. We also dedicate a separate section to the validation of the EM modeling codes used in our simulations.

This report is organized as follows: section 2 explains the modeling methods, both for EM analysis and SAR image formation; section 3 presents the numerical results for the scenarios mentioned above; and section 4 presents conclusions and indicates future directions of research.

2. Modeling Methods

2.1 Electromagnetic Modeling

The EM models performed in this report are based on two different codes: AFDTD (*7*), which implements the finite-difference time-domain (FDTD) technique, and Xpatch (*8*), which is a combination of ray tracing and physical optics (PO). These codes were introduced in our previous modeling work (*2*), and comprehensive descriptions of the underlying computational methods can be found in references 9–10. AFDTD was developed at ARL and implements an "exact" computational electromagnetic (CEM) method, whereas Xpatch was developed by Science Applications International Corporation (SAIC) under a grant from the U.S. Air Force and implements an "approximate" EM solver. AFDTD is a very computationally intensive code both in terms of central processing unit (CPU) time and memory, which makes Xpatch an attractive approach for rapid modeling of very complex problems. The application of these programs to modeling scenarios relevant to STTW radar was extensively validated in our previous studies (*2–3*). In this report, we continue that validation work by comparing SAR images of the complex room obtained by the two CEM methods.

The SAR imaging of targets involves acquiring the radar signature of those targets for various angles and frequencies. AFDTD can obtain the target signature over a large range of frequencies in one run, but each aspect angle involves a separate simulation. All the models (performed with both AFDTD and Xpatch) calculate the monostatic far-field radar signature for plane-wave incidence at a specific pair of azimuth and elevation angles. For a large computational mesh such as the one describing the complex room, the parallel version of the AFDTD code was run at the ARL and U.S. Air Force Research Laboratory (AFRL) Major Source Resource Centers (MSRC) (*11–12*) on High Performance Computing (HPC) systems. For one AFDTD run, we used 128 processors. We used ~500,000 CPU hours to obtain a typical SAR image of the complex room (apertures on both sides of the building, one polarization) with the AFDTD code. Xpatch is a much more efficient code (typically 100 to 1000 faster than AFDTD for a similar problem). It took ~2,000 CPU hours to obtain the far-field data for one room image with Xpatch. The SAR images in this report were created by the Pioneer RCS software.

2.2 Computational Meshes

For this study, we created the computer model of a complex room, containing humans and furniture objects, with overall dimensions of 10 m by 7 m by 2.2 m. Two representations of the computational mesh are shown in figure 1. In creating the mesh, we started with realistic CAD models of the objects and people that were part of the scene. Thus, the exterior walls were made of 0.2-m-thick bricks and were equipped with glass windows and a wooden door. There was also an interior wall made of 5-cm-thick sheetrock (equipped with a door, as shown in figure 1).

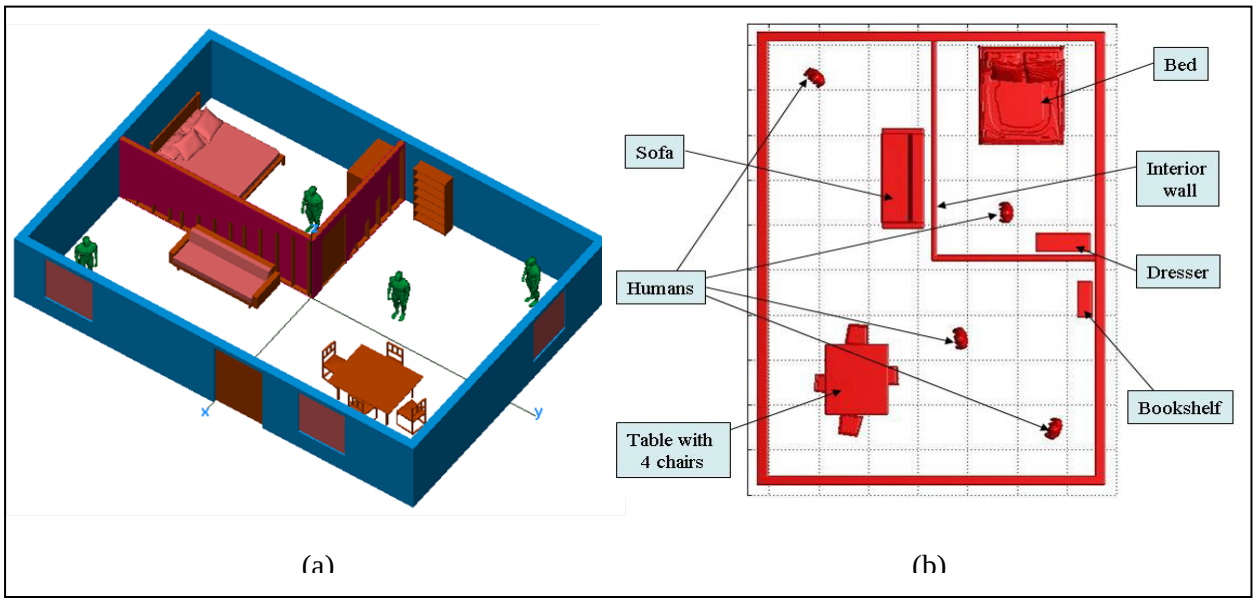

Figure 1. Complex room containing humans and furniture objects showing the (a) perspective view and (b) top view.

We added the following furniture objects: a bed, a couch, a bookshelf, a dresser, and a table with four chairs. These objects were made primarily from wood (except for the mattress and cushions where we used some generic fabric material). We also included 5-cm-thick concrete slabs as ceiling and floor. The dielectric properties of all the materials involved in this study were based on references 13–16 and are listed in table 1. Notice that AFDTD implements a frequency-independent-conductivity model for the dielectric loss, whereas Xpatch implements a dielectric loss model where the imaginary part of the complex permittivity is frequency-independent. Therefore, the σ column in table 1 applies to the AFDTD models, whereas the ε'' column applies to the Xpatch models.

Table 1. Dielectric constant and conductivity of the materials involved in the complex room in figure 1.

Material	ε_r	σ **(S/m)**	ε''
Brick	3.8	0.02	0.24
Concrete	6.8	0.1	1.2
Glass	6.4	0	0
Wood	2.5	0.004	0.05
Sheetrock	2.0	0	0
Fabric	1.4	0	0
Human body	50	1.0	12

There are four humans in this mesh, placed at different azimuth orientation angles. Using the numbering system in figure 1b, the orientation angles are as following: $\phi_1 = 45°$, $\phi_2 = 0°$, $\phi_3 = –20°$, and $\phi_4 = 10°$ (Note: The $\phi = 0°$ angle corresponds to the human facing along the positive *x* direction; the positive angles correspond to a counterclockwise rotation in the horizontal plane). The human meshes represent the "fit man" introduced in a previous study (*1*). Since this model does not include the internal structure of the body, but only the exterior shell, we must assume that the entire body is made of the same uniform dielectric material (see reference 1 for a discussion of the uniform dielectric human body model's validity). For this material dielectric, we picked properties close to those of skin.

In the simulations where we use plane-wave excitation at 0° elevation, the room is placed in free-space, meaning there is no infinite ground plane that extends beyond the room's footprint. This is dictated by the fact that a plane wave propagating at 0° elevation in the presence of an infinite ground plane would produce null total fields everywhere in the space. However, for the simulations of an airborne system, when the elevation angle is 20°, we must add an infinite dielectric ground plane in order to include the ground bounce of the radar waves.

The maximum frequency considered in the simulations is 2.5 GHz. The FDTD cell size is set at 5 mm, meaning that at the highest frequency, the spatial sampling rate in free-space is 24. We chose to oversample the transient fields in order to keep the numerical dispersion errors under control (*9*). Note, however, that inside the wall material ($\varepsilon_r = 3.8$), there are only about 12 samples per wavelength. The FDTD grid involves about 1500 by 2000 by 500 cells, or a total of ~1.68 billion cells. In terms of the frequency and angular steps we use $\Delta f = 6.67$ MHz and $\Delta\phi = 0.25°$. These values ensure that we sample the bandwidth and aperture adequately in order to avoid aliasing in the SAR image creation process (*3*).

2.3 SAR Imaging Algorithm

In a previous study (*3*), we made a detailed introduction of SAR imaging algorithms as applied to STTW radar applications. In that report, we discussed the differences between the spotlight and strip-map data collection geometries (*17–19*), between the near-field and far-field configurations, and between the polar format and backprojection image formation algorithms (*17–19*). All those considerations also apply to the models presented in this report.

Specifically, in section 3, we simulate the spotlight geometry with the radar placed in the far field and use the polar format algorithm (PFA) to create the SAR images. A schematic representation of the spotlight SAR configuration is shown in figure 2, where two separate synthetic apertures are created along two sides of the building. The radar sensor can be mounted on a ground platform, at 0° elevation, or on an airborne platform (for which we consider an elevation angle of 20°). The two-dimensional (2-D) SAR images are created in the slant plane (*17*), which has a tilt equal to the elevation angle with respect to the horizontal plane. Reference 3 discusses the fact that a spotlight SAR operating under the far-field assumption is not necessarily a realistic scenario for current STTW radar system implementation. Nevertheless,

our simulations from that study (*3*) proved that this type of model produces images in good agreement with more realistic scenarios. Additionally, the spotlight-far-field geometry is much more convenient from a computational complexity standpoint.

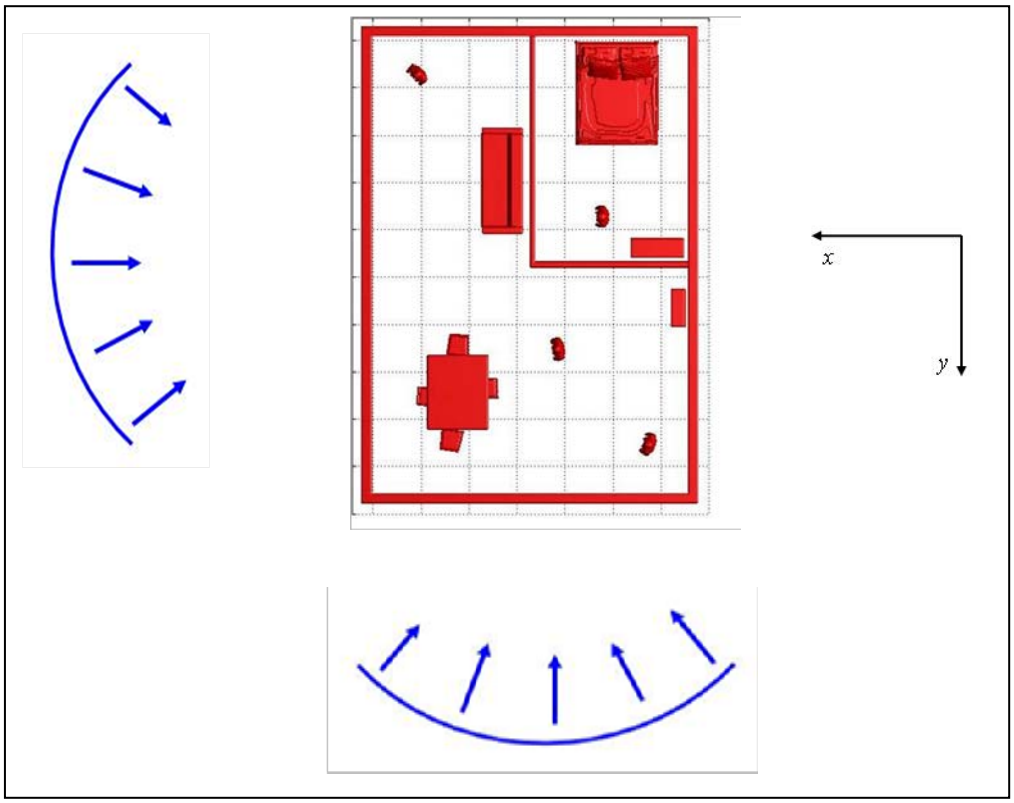

Figure 2. Spotlight SAR geometry implemented by the models in this report, showing two possible aperture positions.

The PFA converts the data format in the frequency-angle domain from polar to Cartesian coordinates and then takes an inverse 2-D Fast Fourier Transform (FFT). This is a computationally efficient procedure, but requires certain imaging geometries to minimize the imaging errors. Thus, placing the radar in the far-field is crucial in eliminating the range curvature effect (*17–18*). Our modeling method automatically satisfies this condition.

One important processing step in the PFA is the polar-to-Cartesian data interpolation (*17–18*). This issue has been previously discussed in detail and illustrated with numerical examples (*3*). In section 3, all the images use the midpoint interpolation method, which achieves a good compromise between high cross-range resolution and sidelobe mitigation. We also make sure we limit the aperture size to no more than 30°, in order to keep the grid conversion error under control (*18*).

The images are presented as magnitude maps in dB scale. The absolute values on the dB scales are not relevant to our analysis. However, the intensity of each image pixel is always scaled back to the number of data points in the 2-D FFT, such that we can perform a meaningful comparison between pixel intensities of images obtained from data sets with different numbers of data points.

The image resolution is given by the range of frequencies and angles considered in the 2-D FFT according to the following equations (*17*):

$$down\text{-}range\ resolution = \frac{c}{2BW} \tag{1}$$

$$cross\text{-}range\ resolution = \frac{\lambda}{2(\phi_{\max} - \phi_{\min})} \tag{2}$$

where c is the speed of light, BW is the radar bandwidth, λ is the wavelength at the center frequency, and $\phi_{\max} - \phi_{\min}$ is the angular aperture (in radians).

In order to reduce the image sidelobes, we use Hanning windows (*20*) in both the frequency and the angular domains. The windowing procedure reduces the resolution as compared to the image that would use the full aperture and bandwidth—by about a factor of 2. In section 3, the bandwidth and aperture sizes are listed as "effective" bandwidth/aperture (*21*). One should keep in mind that the underlying data in terms of frequencies or angles extends twice as much as the effective bandwidth/aperture.

It is important to mention that, throughout this report, the image formation algorithm does not attempt to compensate for the delays caused by propagation through walls. This makes the images of targets placed in a room appear at a location behind their real position, in addition to making them slightly de-focused. This effect could be more severe for wall materials with large dielectric constant such as concrete. Section 3 discusses the implications of this artifact, which occurs when combining images from different aspect angles. Techniques for compensating for the wall delays in through-the-wall radar images are beyond the scope of this report.

3. Numerical Results

3.1 SAR Images from a Ground-based Radar System

First, we present the images in a scenario simulating a ground-based radar platform, where the elevation angle is 0° (propagation vector in the *x-y* or horizontal plane). Figure 3 shows the images obtained for vertical-vertical (V-V) polarization with an aperture centered at the (a) left and (b) bottom of the page. As expected, if the aperture includes the direction perpendicular to a wall, that wall appears prominently in the image. The human targets also show up in the images, but they would be more difficult to detect because of the increased clutter (compared to the simple room). Notice that the human images are brighter when they are located directly behind a window or door. The furniture objects appear generally weaker than the human targets, with the notable exception of the bookshelf when the aperture is placed on the left side. The reason for the weak scattering from the furniture objects is the low dielectric constant of wood (which all the

furniture in our scene is made of). However, metallic furniture objects could produce signatures that are at least as strong as the human targets (see reference 3 for an example), possibly confusing a radar detection scheme for stationary targets.

Figure 4 presents the images obtained for horizontal-horizontal (H-H) polarization with the same aperture placements as in figure 5. It is apparent by comparing the two sets of images that there is no major difference between the H-H and V-V polarizations for incidence at 0° elevation. This is consistent with our previous findings (*1–3*).

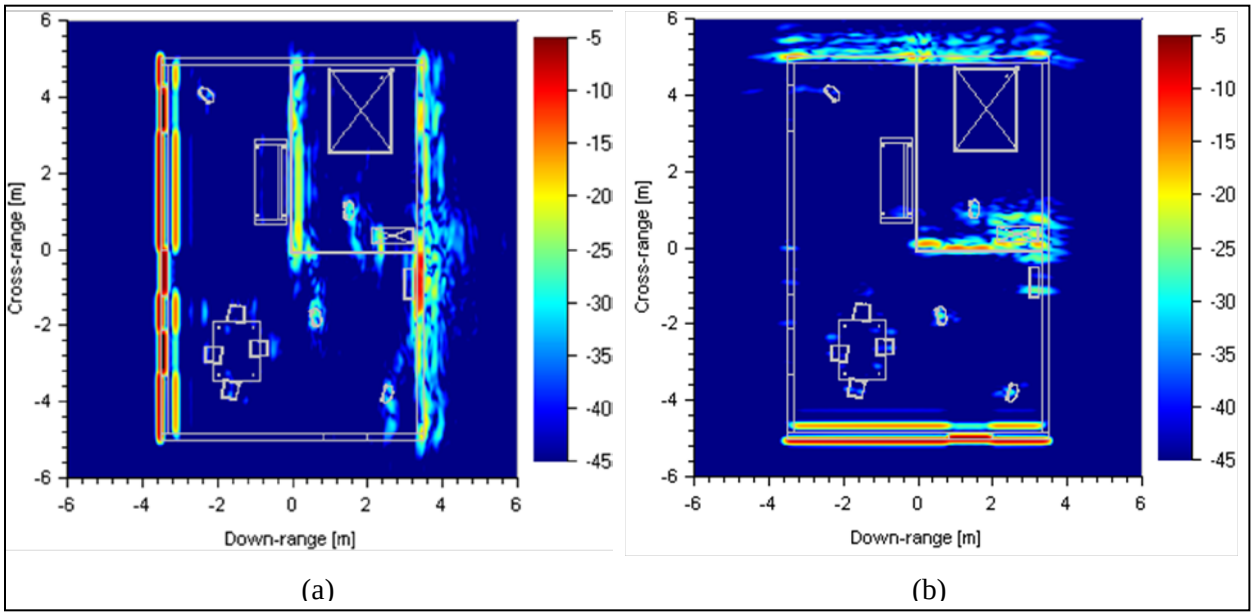

Figure 3. SAR images of the complex room, obtained for spotlight mode and PFA from AFDTD data in V-V polarization, 0° elevation, 1.1 GHz bandwidth centered at 1.4 GHz, for a 30° synthetic aperture placed on the (a) left side and (b) bottom side.

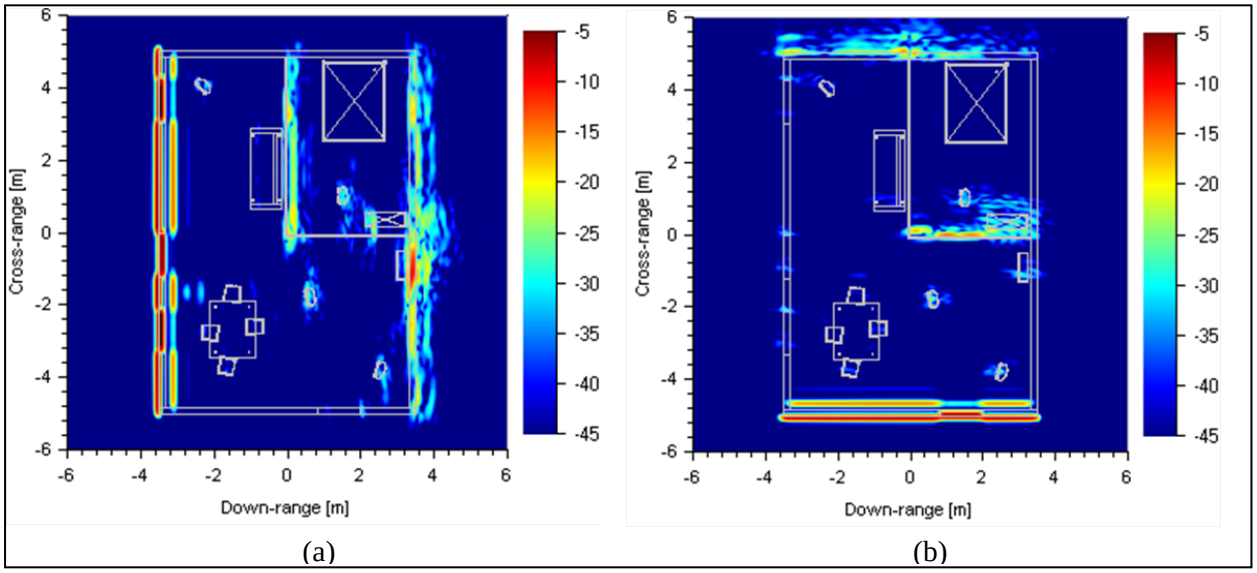

Figure 4. SAR images of the complex room, obtained for spotlight mode and PFA from AFDTD data in H-H polarization, 0° elevation, 1.1 GHz bandwidth centered at 1.4 GHz, for a 30° synthetic aperture placed on the (a) left side and (b) bottom side.

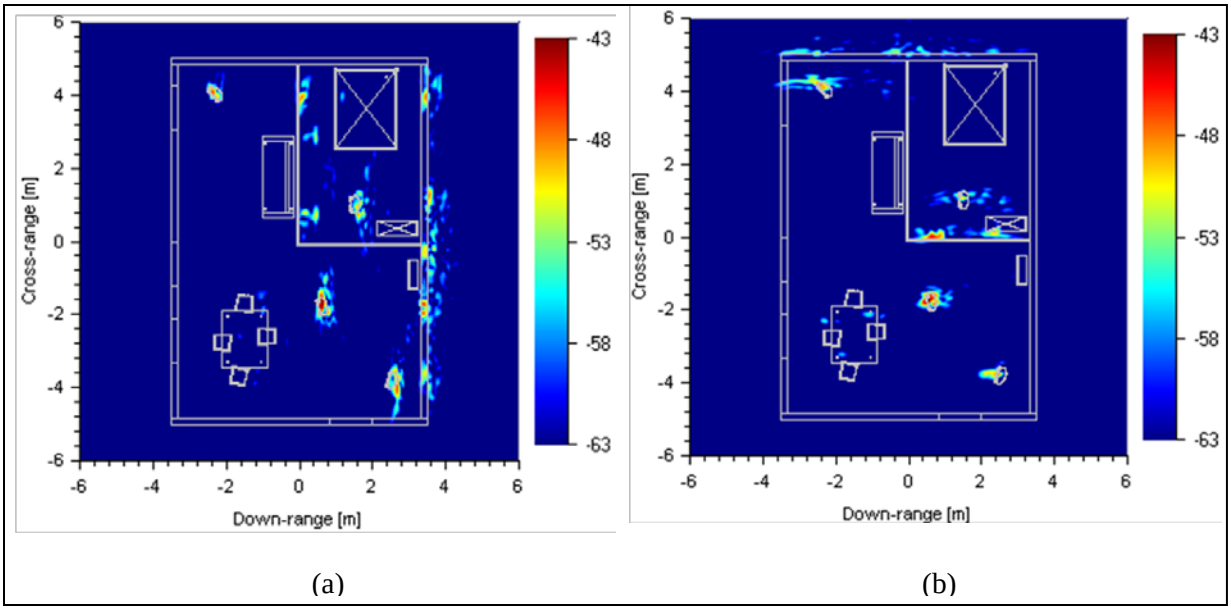

Figure 5. SAR images of the complex room, obtained for spotlight mode and PFA from AFDTD data in V-H polarization, 0° elevation, 1.1 GHz bandwidth centered at 1.4 GHz, for a 30° synthetic aperture placed on the (a) left side and (b) bottom side.

3.2 Using Cross-polarization for SAR Imaging

It was suggested and demonstrated on simple scenarios (*3*) that operating the radar in cross-polarization can enhance the human targets in a SAR image, while suppressing the walls and possibly other clutter objects. Our simulations performed on the complex room confirm this idea. Thus, figure 3 shows the SAR images of the complex room obtained for vertical-horizontal (V-H) polarization, from the (a) left and (b) bottom of the page. In this case, the human targets are very bright compared to both the walls and the furniture objects (most of these have regular shapes with straight edges). Interestingly, about the only other bright objects in the cross-polarization images are the "ghost" images of the humans, which appear at the projection points on the back walls (notice that one human may project on more than one wall, creating multiple ghosts). A detailed analysis of this phenomenon was presented in reference 3.

3.3 Combining SAR Images from Different Aspect Angles

To obtain the complete room layout, a natural step is to combine the two images in figures 3 through 5 obtained from two orthogonal sides of the building. We demonstrate that in figure 6, where we incoherently add the V-V polarization images (figure 6a) and the V-H polarization images (figure 6b). Notice that the combination consists of pixel-by-pixel addition of image magnitudes, performed in the linear space (not in dB). The image in figure 6a displays the entire building layout. However, recall that the targets inside the room are slightly displaced from their real location in both images in figure 3. Moreover, these displacements are in different directions, meaning that when we combine the two images, the target smearing is increased (while the effective target resolution is degraded). This becomes more evident in figure 6b,

where only the human targets (and their ghosts) show clearly in the image. As a consequence, the image addition procedure is beneficial for the purpose of mapping the building layout (using co-polarized images), but does not add any advantage in detecting the targets inside—in fact, most likely the detection performance decreases. This result clearly reveals a shortcoming of creating SAR images of the room without compensating for the propagation delays through the walls.

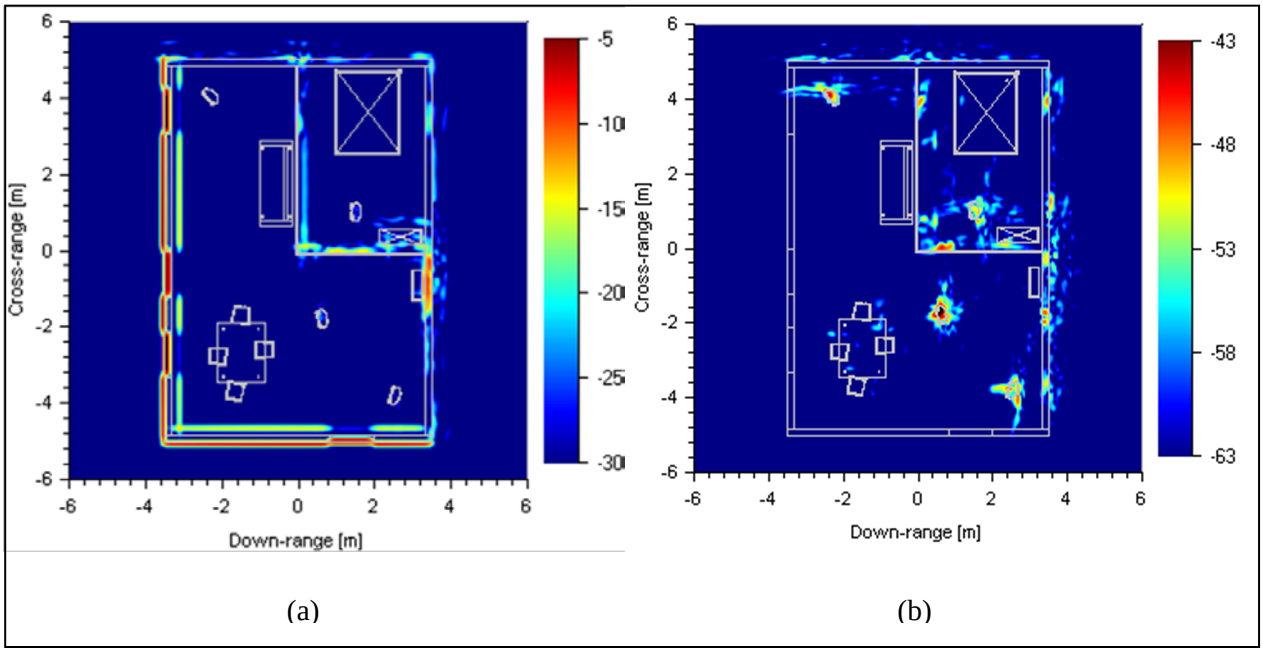

Figure 6. Incoherent pixel-by-pixel summation of the co-polarized images from both sides of the building showing (a) V-V and (b) V-H polarization.

If the goal is to detect targets inside a room, there are more effective ways to fuse images obtained from different viewpoints. Ahmad and Amin (*22*) presented a procedure where the image magnitudes were multiplied pixel-by-pixel in the linear space (addition in dB). This process emphasizes targets that are fairly isotropic in azimuth (those that appear with reasonable brightness in the images taken from both viewpoints) and minimizes the response of targets displaying strongly angular-dependent scattering (those that appear brightly from only one viewpoint). Human targets belong to the first category, whereas walls belong to the second. This process can be further enhanced through a gamma correction, where the magnitude of each image pixel is raised to a power g prior to multiplication. For $g > 1$, the image contrast is increased. As shown by Ahmad and Amin (*22*), this process could improve target detection performance. A key prerequisite for making this procedure work is obtaining the correct location of the targets in each separate image. The SAR image formation algorithm described in Ahmad and Amin (*22*) achieves that by assuming that the wall parameters are known and computing the exact propagation delays between each pixel and each aperture sample position. Also worth mentioning is the fact that the pixel-by-pixel image multiplication procedure would eliminate the ghosts in a multi-view combined image.

Revisiting the idea of adding images from two orthogonal viewpoints, we notice that we can also combine images obtained in different polarization modes (after an appropriate rescaling of the magnitudes). Thus, in figure 7, we add the V-V images obtained from two building sides and the V-H image obtained from only one side (left in figure 7a and bottom in figure 7b). Notice that we do not add the cross-polarization images from both sides in order to avoid the smearing effect created by the wrong target localization. The V-H images are amplified by 30 dB before summation. The resulting images create both the building footprint and bright images of the humans. Although the latter are still slightly displaced, their resolution is as good as in the original one-side images (notice that the V-V images of the humans play almost no role in the newly combined image).

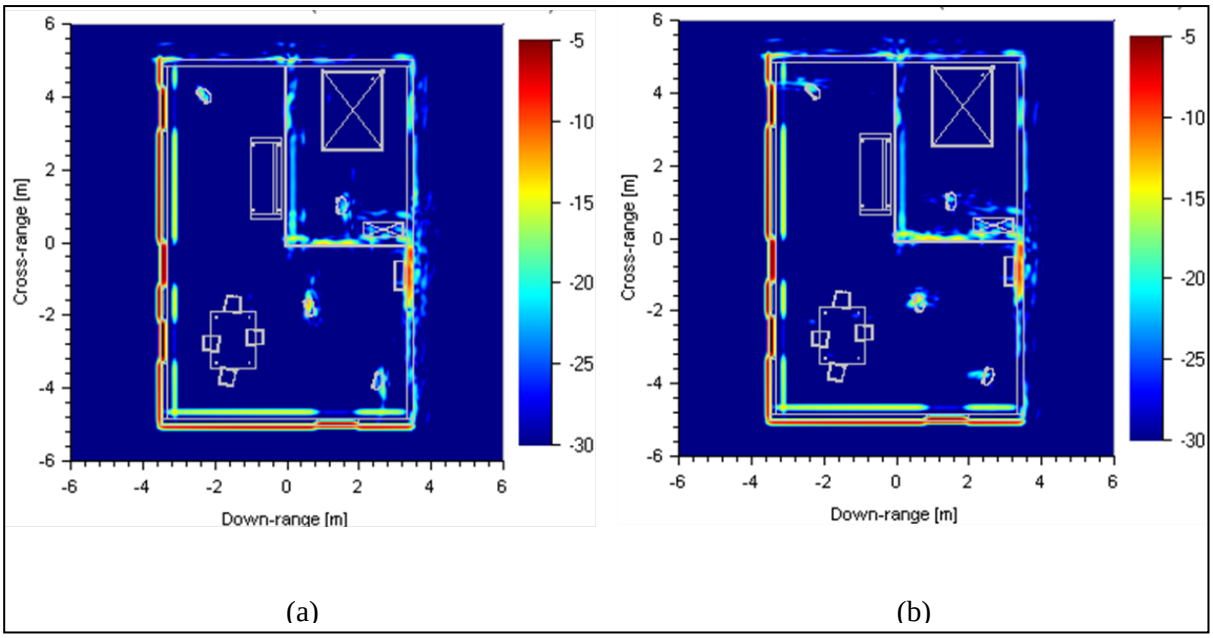

Figure 7. Incoherent pixel-by-pixel summation of the V-V images from both sides of the building and the V-H image from (a) the left side of the building and (b) the bottom side of the building.

Note: The cross-polarization images were amplified by 30 dB before summation.

3.4 SAR Images from an Airborne-based Radar System

To simulate an imaging scenario from an airborne radar platform, we consider incidence at an elevation angle of 20° with respect to the *x-y* or horizontal plane. We keep the assumptions that the radar operates monostatically in the far-field, transmitting and receiving plane waves in a spotlight SAR configuration. In fact, an airborne radar platform could more likely achieve this type of imaging geometry than a ground-based system. For this case, we add an infinite dielectric ground plane with the dielectric properties of concrete $\varepsilon_r = 6.8$ and $\sigma = 0.1$ S/m. The SAR image is built in the slant plane, which now has a 20° tilt with respect to the horizontal.

The images obtained from separate apertures located on two sides of the building are shown in figures 8 (V-V polarization) and 9 (H-H polarization). The combined images for each polarization are shown in figure 10. A striking feature in these figures is represented by the double images of the front wall: the first line corresponds to diffraction off the top edge of the wall; whereas, the second corresponds to the inner corner formed by wall and ground plane (fainter lines corresponding to the back side of the wall are also present in between). Considering the plane-wave excitation, the entire wavefront backscatters coherently from the ground-wall corner via a double reflection, resulting in a large radar return at broadside azimuth incidence.

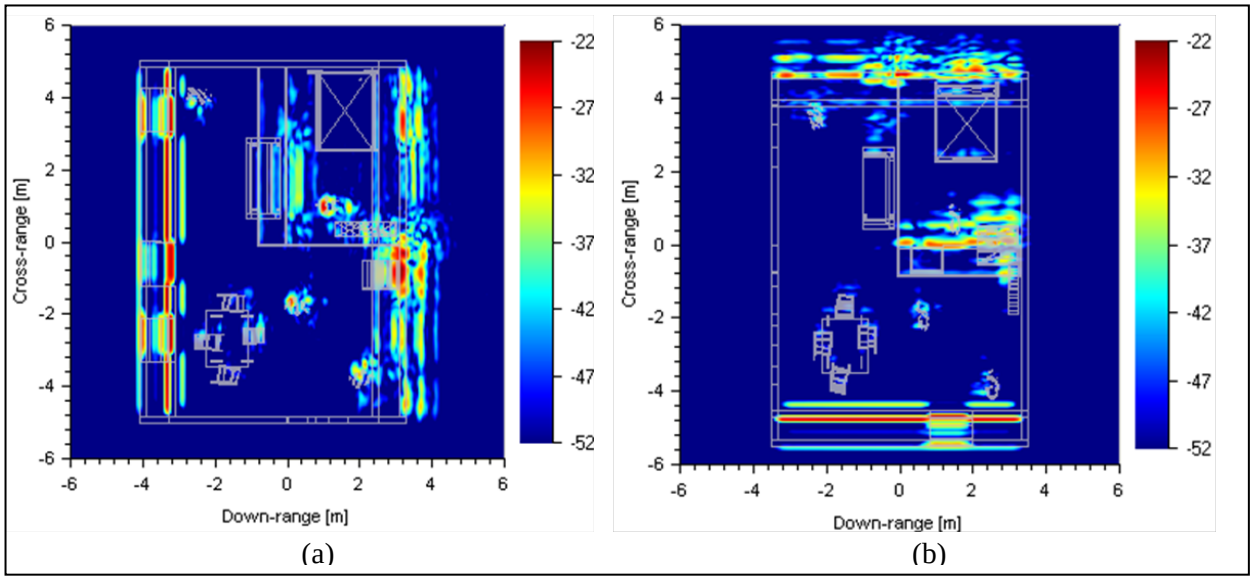

Figure 8. SAR images of the complex room, obtained for spotlight mode and PFA from AFDTD data in V-V polarization, 20° elevation, 1.1 GHz bandwidth centered at 1.4 GHz, for a 30° synthetic aperture placed on the (a) left side and (b) bottom side.

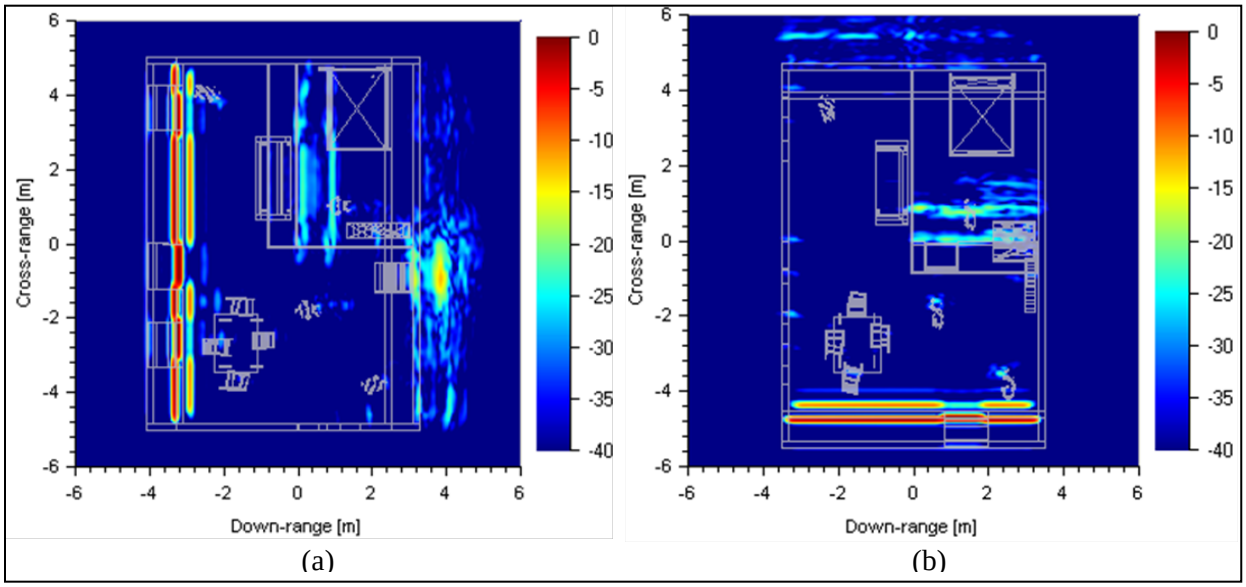

Figure 9. SAR images of the complex room, obtained for spotlight mode and PFA from AFDTD data in H-H polarization, 20° elevation, 1.1 GHz bandwidth centered at 1.4 GHz, for a 30° synthetic aperture placed on the (a) left side and (b) bottom side.

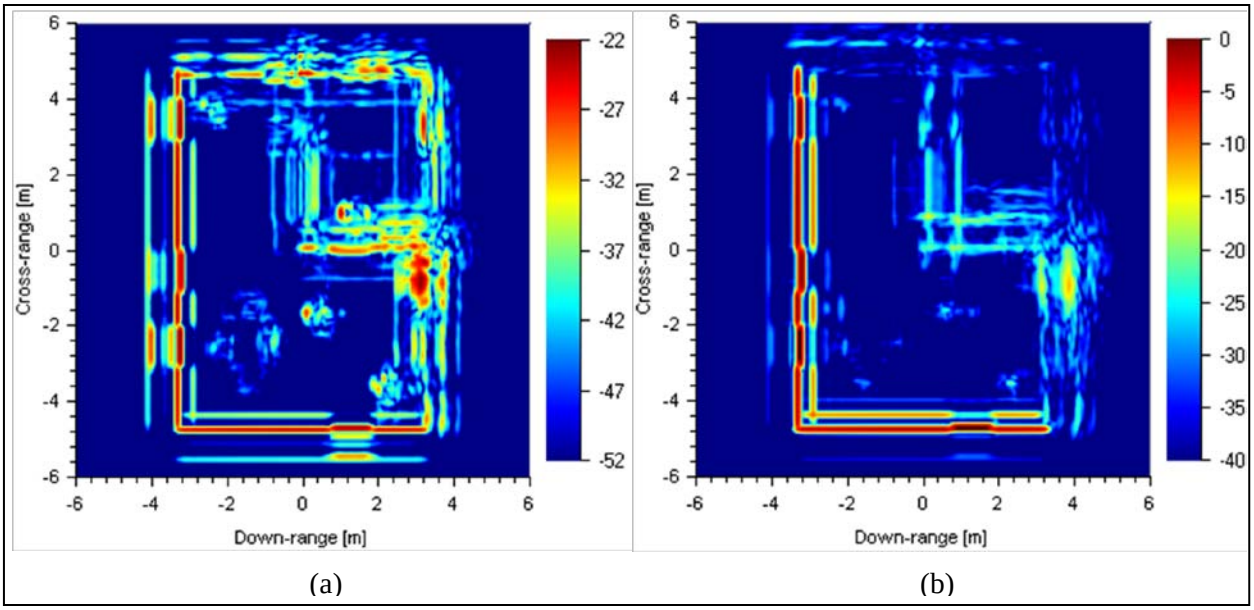

Figure 10. Composite SAR images of the complex room, obtained for spotlight mode and PFA from AFDTD data, 20° elevation, 1.1 GHz bandwidth centered at 1.4 GHz, scanning from two building sides with a 30° synthetic aperture, showing (a) V-V and (b) H-H polarization.

Note: The dynamic ranges are different in the two cases.

However, there is a significant difference in the ground reflection (and consequently, the brightness of the second wall return) between the V-V and H-H polarizations (notice that the H-H image dB scale is 22 dB above the V-V). The difference comes primarily from the presence of the Brewster angle (*23*) in V-V polarization (for this case, the Brewster angle is about 21° from the horizontal, which is almost the same as our incidence elevation angle). This effect strongly reduces the ground reflection of the radar waves. Notice that because of the large dB-scale difference between the V-V and H-H images, most other targets besides the front wall appear relatively weak in the H-H image. However, in absolute terms, they are as bright as (or may be even brighter than) their V-V counterpart.

We also analyzed the cross-polarization images obtained at 20° elevation. For this geometry, the horizontal wall edges project at an oblique angle onto a plane perpendicular to the direction of propagation and create cross-polarized scattered field. Nevertheless, since most of the cross-polarized energy diffracted by these edges scatters forward and only very little in backscatter, this effect should not have a significant impact on the SAR image. In fact, only discontinuities along the horizontal edges should appear in the cross-polarization SAR images (the effect should be stronger as the elevation angle increases). Figure 11 confirms this hypothesis, both for viewing angles from the (a) left and (b) bottom. Most of the bright spots in this image represent small corners formed by the windows, doors, or wall joints. Nevertheless, it appears that this imaging mode is not particularly favorable for detecting the in-room human targets.

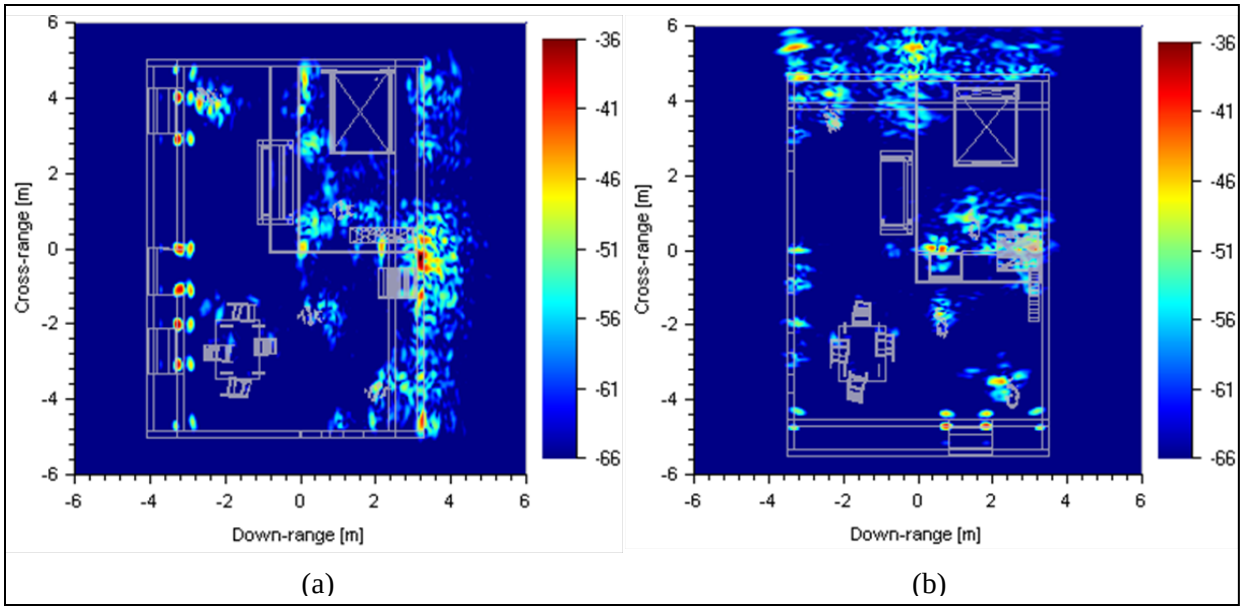

Figure 11. SAR images of the complex room, obtained for spotlight mode and PFA from AFDTD data in V-H polarization, 20° elevation, 1.1 GHz bandwidth centered at 1.4 GHz, for a 30° synthetic aperture placed on the (a) left side and (b) bottom side.

3.5 Comparison between AFDTD and Xpatch Models

We compare the AFDTD- and Xpatch-based images of the complex room in figures 12 and 13. In these figures, we show only the two-side combined images without the mesh overlays. Figure 12 considers an elevation of 0°; whereas, in figure 13, the elevation angle is 20°. For both cases, we look at V-V and H-H polarizations (we do not attempt to compare the cross-polarization results, since we do not expect Xpatch to provide accurate predictions in that case).

For an easy-to-interpret quantitative comparison between the two sets of images (AFDTD versus Xpatch), we tabulate the pixel intensity at all the numbered locations marked in figure 12a for all the elevation angles and polarization combinations considered in this section in table 2. The maximum pixel intensity is recorded for each of these areas. Points 1–4 sample images of front walls (front and back edges) and are representative for the wall reflection and transmission phenomena (notice that a window is placed at points 3 and 4). The points 5–8 were picked in the areas where the four humans are placed, since they are most likely the targets of interest in a STTW scenario. We also chose point 9 at the room's far corner, where diffraction phenomena are important. A discussion on the relevance of such comparisons for SAR images obtained by various methods has been published elsewhere (*3*).

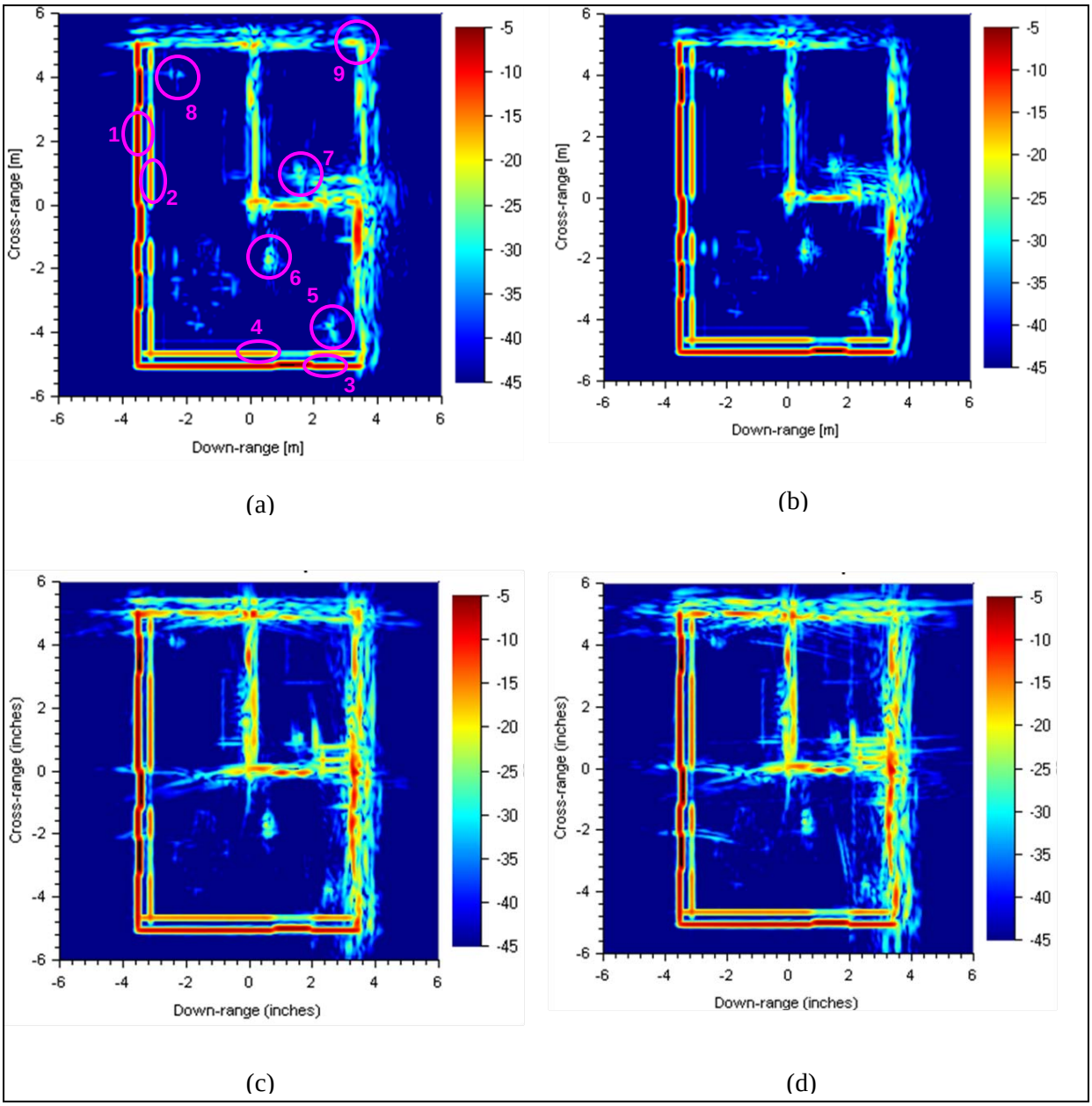

Figure 12. Composite SAR images of the complex room, obtained for spotlight mode and PFA, 0° elevation, 1.1 GHz bandwidth centered at 1.4 GHz, scanning from two building sides with a 30° synthetic aperture, showing (a) V-V polarization, AFDTD data; (b) H-H polarization, AFDTD data; (c) V-V polarization, Xpatch data; and (d) H-H polarization, Xpatch data.

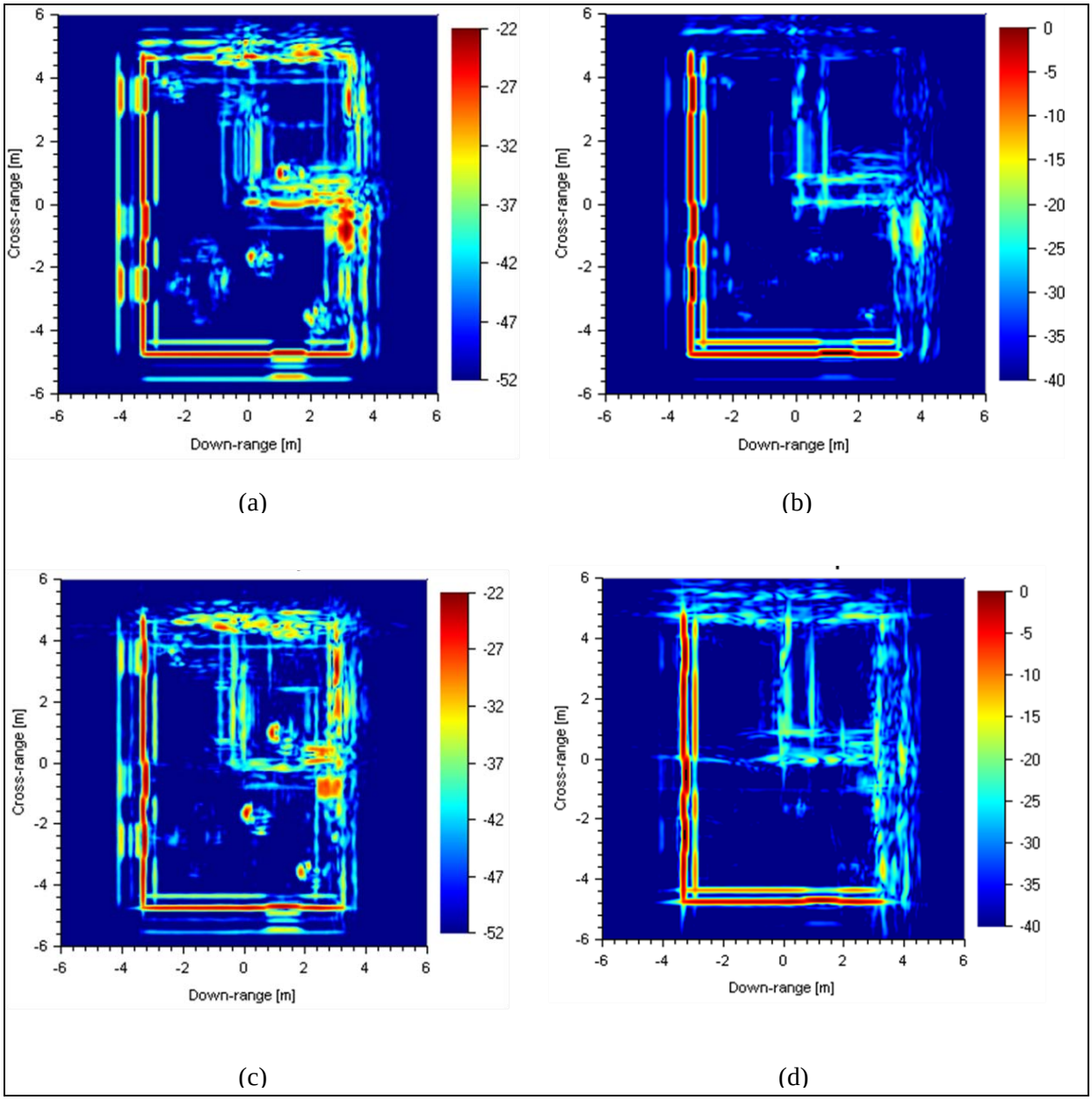

Figure 13. Composite SAR images of the complex room, obtained for spotlight mode and PFA, 20° elevation, 1.1 GHz bandwidth centered at 1.4 GHz, scanning from two building sides with a 30° synthetic aperture, showing (a) V-V polarization, AFDTD data; (b) H-H polarization, AFDTD data; (c) V-V polarization, Xpatch data; and (d) H-H polarization, Xpatch data.

Table 2. Comparison between AFDTD and Xpatch imaging results at the points highlighted in figure 12a for all the images considered in section 3.5 (data in dB). The bottom row contains the cross-correlation between the images created by the two methods.

Elevation	**0°**				**20°**			
Polarization	**V-V**		**H-H**		**V-V**		**H-H**	
Code	FDTD	Xpatch	FDTD	Xpatch	FDTD	Xpatch	FDTD	Xpatch
1	–10.4	–10.6	–10.5	–10.7	–28.6	–28.7	–5.9	–6.0
2	–19.3	–18.0	–19.3	–18.1	–39.3	–39.7	–14.6	–13.6
3	–9.3	–10.0	–9.3	–10.0	–28.0	–28.2	–5.0	–5.7
4	–31.7	–29.3	–32.8	–29.2	–	–	–27.8	–25.9
5	–27.4	–26.2	–26.6	–27.9	–32.8	–31.9	–22.4	–30.6
6	–24.0	–21.9	–24.3	–22.1	–30.4	–29.7	–27.1	–27.4
7	–25.4	–26.8	–26.8	–27.8	–28.2	–29.2	–	–
8	–31.2	–28.6	–30.1	–28.9	–35.4	–36.9	–28.0	–33.4
9	–17.4	–11.5	–27.6	–18.4	–30.5	–31.5	–30.7	–22.8
Correlation	0.945		0.933		0.844		0.976	

By looking at the numbers in table 2, we notice good match between the Xpatch and AFDTD results for the points 1–8 for almost all the cases considered, with the differences rarely exceeding 2 dB. Some exceptions are noticed for the human targets at 20° elevation and H-H polarization, where the humans show up very weakly in the images as compared to the walls (and therefore, this case would be very unfavorable for a through-the-wall human target detection scheme). Notice that, in some cases, we were not able to record the pixel intensity of specific objects in the image (especially at 20° elevation) because those object images were completely overlapped by other features with larger intensity. More significant differences between the Xpatch and AFDTD results are observed for point 9 (the far corner). The explanation is that Xpatch does not accurately account for corner diffraction at oblique incidence angles, since the PO technique cannot handle this phenomenon by itself (at the same time, a geometric theory of diffraction formula for dielectric wedges is not available [*10*]). A more detailed analysis of these errors based on electromagnetic phenomenology has been presented elsewhere (*2*).

While comparing the maximum pixel intensity in specific areas of interest of the image represents a localized measure of code accuracy, we can also perform a global comparison by computing the cross-correlation of the images obtained by the two methods. Note that the cross-

correlation is computed pixel-by-pixel between the magnitudes of the SAR images. A more accurate correlation method would consider the complex SAR images and take the pixel-by-pixel product and sum of one image and the complex conjugate of the other. However, the complex pixel tables of the SAR images presented in this report were not available to us. The results in table 2 demonstrate very good correlation between the images obtained by AFDTD and Xpatch.

4. Conclusions

In this work, we reported simulations of a SAR system for large and complex building imaging. While the large-scale computer models performed here constitute an achievement on their own, our emphasis was primarily on studying the phenomenology involved in this radar scenario, as well as suggesting techniques for enhancing image quality and behind-the-wall target detection.

Based on a recent review of open literature, all the current testbed STTW radar imaging systems are ground-based platforms (*4, 24–26*).Therefore, we dedicated a significant part of our analysis to this type of scenario. Although we did not notice significant differences between V-V and H-H polarizations in this case, we showed that operating the radar in cross-polarization leads to interesting effects that may enhance the chances of detecting human targets in a room. We also investigated modalities of combining images from different aspect angles in order to obtain the entire room layout. When both co- and cross-polarization images are overlaid on the same pixel map (after appropriate renormalization), the humans appear prominently, together with the walls and other strong scatterers. These findings make the case for implementing a fully polarimetric radar for STTW applications. Moreover, as shown previously in another study (*27*), polarimetric image data can be employed in detecting small weapons carried by humans.

Future radar systems may attempt to create building images from airborne platforms. We investigated such a scenario in section 3.4. In this case, we noticed significant differences between the V-V and H-H polarizations, particularly related to the ground bounce of the radar waves. Because of this effect, the receiver of a radar operating in H-H polarization would require a much larger dynamic range than that of a V-V polarized radar, when the elevation angle is close to the Brewster angle. Additionally, we did not notice any particular advantage in employing the cross-polarization mode for this scenario.

Finally, we analyzed the accuracy of the EM simulation codes, AFDTD and Xpatch, by directly comparing the SAR images based on model-generated data. The agreement was generally very good, although Xpatch displayed some errors in certain image regions (particularly at the room's corners).

One phenomenon that can introduce false detections in a STTW radar system is the ghost image caused by multipath propagation and scattering of radar waves. The techniques described in this report did not address this issue, which will be investigated in future studies of STTW imaging

systems. Other future work will include adding more complexity to the building models, such as pipes, wires, roof beam structures, and heating-ventilation ducts. Eventually, some scenarios will have to address multi-story buildings. In all these situations, the vertical separation of various features would be the key to detecting specific targets. Therefore, three-dimensional imaging systems will need to be developed for this purpose. Simulating such radar systems will be one prominent item in our future research.

5. References

1. Dogaru, T.; Nguyen, L.; Le, C. *Computer Models of the Human Body Signature for Sensing Through the Wall Radar Applications*; ARL-TR-4290; U.S. Army Research Laboratory: Adelphi, MD, September 2007.

2. Dogaru, T.; Le, C. *Simulated Radar Range Profiles of Simple Room as Computed by FDTD and Xpatch*; ARL-TR-4420; U.S. Army Research Laboratory: Adelphi, MD, April 2008.

3. Dogaru, T.; Le, C. *SAR Images of a Simple Room Based on Computer Models*; ARL-TR-5193; U.S. Army Research Laboratory: Adelphi, MD, May 2010.

4. Nguyen, L.; Ressler, M.; Sichina, J. Sensing Through the Wall Imaging Using the Army Research Lab Ultra-wideband Synchronous Impulse Reconstruction (UWB SIRE) Radar. *Proceedings of SPIE* **2008**, *6947*.

5. Le, C.; Dogaru, T.; Nguyen, L.; Ressler, M. Ultra-wideband (UWB) Radar Imaging of Building Interiors: Measurements and Predictions. *IEEE Transaction on Geophysics and Remote Sensing* **May 2009**, *47*, 1409–1420.

6. Martone, A.; Innocenti, R.; Ranney, K. *Moving Target Indication for Transparent Urban Structures*; ARL-TR-4809; U.S. Army Research Laboratory: Adelphi, MD, May 2009.

7. Dogaru, T. *AFDTD User's Manual*; ARL-TR-5145; U.S. Army Research Laboratory: Adelphi, MD, March 2010.

8. Science Applications International Corporation (SAIC) Web page. http://www.saic.com/products/software/xpatch (accessed December 2009).

9. Taflove, A.; Hagness, S. C. *Computational Electrodynamics: The Finite-Difference Time-Domain*: Artech House: Boston, MA, 2000.

10. Ruch, G.; Barrick, D. E.; Stuart, W. D.; Krichbaum, C. K. *Radar Cross Section Handbook*: Plenum Press: New York, 1970.

11. ARL MSRC Web page. http://www.arl.hpc.mil (accessed August 2009).

12. AFRL MSRC Web page. http://www.asc.hpc.mil (accessed August 2009).

13. Pena, D.; Feick, R.; Hristov, H.; Groto, W. Measurement and Modeling of Propagation Losses in Brick and Concrete Walls for the 900-MHz Band. *IEEE Transactions on Antennas and Propagation* **January 2003**, *51*, 31–39.

14. Muqaibel, A.; Safaai-Jazi, A.; Bayram, A.; Attiya, A.; Riad, S. Ultra-wideband Through-the-Wall Propagation. *IEE Proceedings – Microwave, Antennas and Propagation* **December 2005**, *152*, 581–588.

15. Stone, W. *Electromagnetic Signal Attenuation in Construction Materials*; NISTIR 6055; National Institute of Standards and Technology: Gaithersburg, MD, October 1997.

16. Yang, C. F.; Ko, C. J.; Wu, B. C. A Free Space Approach for Extracting the Equivalent Dielectric Constants of the Walls in Buildings. *1996 IEEE Antennas and Propagation International Symposium*, Baltimore, MD, July 1996, 1036–1039.

17. Carrara, W.; Goodman, R.; Majewski, R. *Spotlight Synthetic Aperture Radar – Signal Processing Algorithms*: Artech House: Boston, MA, 1995.

18. Jakowatz, C.; Wahl, D.; Eichel P.; Ghiglia, D.; Thompson, P. *Spotlight-Mode Synthetic Aperture Radar: A Signal Processing Approach*: Kluwer Academic Publishers: Norwell, MA, 1996.

19. Soumekh, M. *Synthetic Aperture Radar Signal Processing*: Wiley: New York, 1999.

20. Oppenheim, A. V.; Schafer, R. W. *Discrete-Time Signal Processing*: Prentice Hall: Englewood Cliffs, NJ, 1989.

21. Shaeffer, J. F.; Hom, K. W.; Baucke, R. C.; Cooper, B. A.; Talcott, N. A. *Bistatic k-space imaging for electromagnetic prediction codes for scattering and antennas*; Technical Paper NASA-TP-3569; National Aeronautics and Space Administration: Langley, VA, July 1996.27.

22. Ahmad, F.; Amin, M. G. Multi-location wideband synthetic aperture imaging for urban sensing applications. *Journal of the Franklin Institute* **September 2008**, *345*, 618–639.

23. Balanis, C. *Advanced Engineering Electromagnetics*: Wiley: New York, 1989.

24. Clark, B. Trial Results of a Stand-off Sense-Through-The-Wall Radar. *Proceedings of the 55th Annual MSS Tri-Service Radar Symposium*, June 2009.

25. Hunt, A. R. Use of a Frequency-hopping Radar for Imaging and Motion Detection Through Walls. *IEEE Transaction on Geophysics and Remote Sensing* **May 2009**, *47*, 1402–1408.

26. Farwell, M.; Ross, J.; Luttrell, R.; Cohen, D.; Chin, W.; Dogaru, T. Sense Through the Wall System Development and Design Considerations. *Journal of the Franklin Institute* **September 2008**, *345*, 570–591.

27. Dogaru, T.; Le, C. *Through-the-Wall Small Weapon Detection Based on Polarimetric Radar Techniques*; ARL-TR-5041; U.S. Army Research Laboratory: Adelphi, MD, December 2009.

List of Symbols, Abbreviations, and Acronyms

2-D	two-dimensional
AFRL	U.S. Air Force Research Laboratory
ARL	U.S. Army Research Laboratory
CAD	computer-aided design
CEM	computational electromagnetics
CERDEC	Communications-Electronics Research Development and Engineering Center
CPU	central processing unit
EM	electromagnetic
FDTD	Finite Difference Time Domain
FFT	fast Fourier transform
H-H	horizontal-horizontal
HPC	high-performance computing
I2WD	Intelligence and Information Warfare Directorate
MSRC	Major Shared Resource Center
PFA	polar format algorithm
PO	physical optics
SAIC	Science Application International Corporation
SAR	synthetic aperture radar
SIRE	Synchronous Impulse Reconstruction radar
STTW	sensing through the wall
V-H	vertical-horizontal
V-V	vertical-vertical

NO. OF COPIES	ORGANIZATION
1 ELECT	ADMNSTR DEFNS TECHL INFO CTR ATTN DTIC OCP 8725 JOHN J KINGMAN RD STE 0944 FT BELVOIR VA 22060-6218
1 CD	OFC OF THE SECY OF DEFNS ATTN ODDRE (R&AT) THE PENTAGON WASHINGTON DC 20301-3080
1	US ARMY RSRCH DEV AND ENGRG CMND ARMAMENT RSRCH DEV & ENGRG CTR ARMAMENT ENGRG & TECHNLGY CTR ATTN AMSRD AAR AEF T J MATTS BLDG 305 ABERDEEN PROVING GROUND MD 21005-5001
1	US ARMY TRADOC BATTLE LAB INTEGRATION & TECHL DIRCTRT ATTN ATCH B 10 WHISTLER LANE FT MONROE VA 23651-5850
2	US ARMY RDECOM CERDEC INTELLIGENCE & INFO WARFARE DIRECTORATE (I2WD) ATTN AMSRD-CER-IW-IM W CHIN ATTN AMSRD-CER-IW-IM M FARWELL BLDG 600, MCAFEE CENTER FT MONMOUTH NJ 07703
1	PM TIMS, PROFILER (MMS-P) AN/TMQ-52 ATTN B GRIFFIES BUILDING 563 FT MONMOUTH NJ 07703
1	US ARMY INFO SYS ENGRG CMND ATTN AMSEL IE TD A RIVERA FT HUACHUCA AZ 85613-5300

NO. OF COPIES	ORGANIZATION
1	COMMANDER US ARMY RDECOM ATTN AMSRD AMR W C MCCORKLE 5400 FOWLER RD REDSTONE ARSENAL AL 35898-5000
1	US GOVERNMENT PRINT OFF DEPOSITORY RECEIVING SECTION ATTN MAIL STOP IDAD J TATE 732 NORTH CAPITOL ST NW WASHINGTON DC 20402
1	US ARMY RSRCH LAB ATTN RDRL CIM G T LANDFRIED BLDG 4600 ABERDEEN PROVING GROUND MD 21005-5066
15	US ARMY RSRCH LAB ATTN RDRL D OFFICE OF DIRECTOR ATTN IMNE ALC HRR MAIL & RECORDS MGMT ATTN RDRL CIM L TECHL LIB ATTN RDRL CIM P TECHL PUB ATTN RDRL SER M W O COBURN ATTN RDRL SER U A MARTONE ATTN RDRL SER U A SULLIVAN ATTN RDRL SER U C LE ATTN RDRL SER U K KAPPRA ATTN RDRL SER U K RANNEY ATTN RDRL SER U L NGUYEN ATTN RDRL SER U M RESSLER ATTN RDRL SER U D LIAO ATTN RDRL SER U T DOGARU (2 COPIES) ADELPHI MD 20783-1197

TOTAL: 26 (24 HCS, 1 CD, 1 ELECT)